Chinese Chemical Letters 35 (2024) 108510

Contents lists available at ScienceDirect

Chinese Chemical Letters

journal homepage: www.elsevier.com/locate/cclet

Mechanistic insights into the processes of the initial stage of electrolyte degradation in lithium metal batteries

Yao Wang[a,b,1], Juncheng Wang[a,1], Jianwei Nai[a], Jianmin Luo[a], Xinyong Tao[a], Yujing Liu[a,*]

[a] College of Materials Science and Engineering, Zhejiang University of Technology, Hangzhou 310014, China
[b] Moganshan Research Institute at Deqing County Zhejiang University of Technology, Huzhou 313000, China

ARTICLE INFO

Article history:
Received 11 March 2023
Revised 29 March 2023
Accepted 26 April 2023
Available online 27 April 2023

Keywords:
Li metal battery
Electrolyte
Solvation structures
Interface
Density functional theory

ABSTRACT

The lithium (Li) metal batteries (LMBs) are considered one of the most promising next-generation batteries due to its extremely high theoretical specific capacity. However, there are a couple of issues, *e.g.*, the serious side reactions that occurred at the solid-liquid interface between the electrolyte and Li metal anode, hindering the broad commercialization of LMBs. Thus, a comprehensive understanding of the mechanisms underlying the decomposition of electrolytes is crucial to the design of LMBs. Herein, we utilize density functional theory simulations to explore the decomposition mechanism of electrolytes. The most commonly used ether electrolyte solvents, *i.e.*, 1,2-dimethoxyethane (DME) and 1,3-dioxalane (DOL), based on suitable lithium salts, namely bis(trifluoromethanesulfonyl)imide (LiTFSI), are chosen to model the actual situations. We explicitly demonstrate that an electron-rich environment near the interface accelerates the decomposition of electrolytes. For ether electrolytes, we show that the LiTFSI degradation path is depending on the ratio of DOL to DME. In addition, the solvation structures of lithium-ion undergo a series of transformations upon electrolyte degradation, becoming thermodynamically more favorable and having a higher reduction potential in an electron-rich environment. Our finding provides new insights into the decomposition mechanisms of electrolytes and paves the way for the rational design of high-performance LMBs.

Recently, lithium (Li) metal batteries (LMBs) have gained more and more attention and are considered to be the next generation of energy storage devices due to the extremely high theoretical specific capacity (3860 mAh/g) and low electrochemical potential (−3.04 V *vs.* the standard hydrogen electrode) [1–3]. However, the commercialization of the LMBs has been a struggle due to safety issues including short-circuit, leakage, or even explosion. The uneven deposition of Li ions during charging and discharging leads to the formation of Li dendrites [4–6], which can pierce the battery separator and cause the above safety concerns. A successful approach to solving such problems is the construction of the artificial solid electrolyte interphase (SEI) layer [7–9], which is the result of electrolyte degradation at the solid-liquid interface between Li metal anode and electrolyte and can effectively suppress the growth of lithium dendrites [10,11]. It is well known that the components of electrolytes are crucial due to the solvation-structure-derived SEI in LMBs [12–15]. Therefore, great efforts have been devoted to optimizing the components of lithium salts and organic solvents [16,17]. Nevertheless, this kind of optimization strategy still lacks rational design and effective theoretical guidance.

For LMBs, ether electrolytes with high ionic conductivity have better reduction stability than carbonates leading to stable SEI [18]. In the conventional ether-based electrolytes, Li bis(trifluoromethanesulfonyl)imide (LiTFSI) is widely used as a lithium salt in 1,2-dimethoxyethane (DME) and 1,3-dioxalane (DOL) solvents for battery systems [19–21]. For these electrolyte components, 1 mol/L LiTFSI in DOL/DME (1:1, v/v) has been screened for superior performance and is regarded as an optimal ratio in the battery field [22,23]. However, the process of the solvation structures decomposition to generate SEI and the effect of the local chemical environment on it is difficult to be elucidated clearly [13,15,24]. Obviously, research on the mechanism of electrolytes decomposition is urgently required to achieve the ideal SEI for high-performance LMBs [2,25].

Traditional experimental techniques have encountered substantial resistance in exploring the above issues due to the air and electron beam sensitivity of Li metal [26]. Fortunately, state-of-art theoretical predictions have been performed to explore novel electrolyte components and the reaction mechanism of electrolyte degradation, avoiding expensive trial-and-error experiments

* Corresponding author.
E-mail address: yujingliu@zjut.edu.cn (Y. Liu).
[1] These authors contributed equally to this work.

https://doi.org/10.1016/j.cclet.2023.108510
1001-8417/

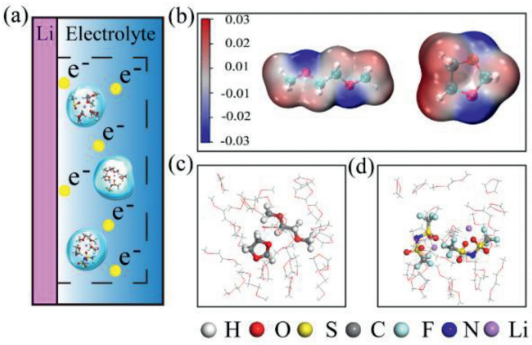

Fig. 1. (a) The model of the electrolyte and Li-metal in electron-rich environment for this work. (b) The electrostatic diagrams (in a.u.) of the DOL and DME. The initial conformations used in the AIMD for (c) mixed DME/DOL. (d) S–N situations. The dotted box in panel (a) represents the modeled systems.

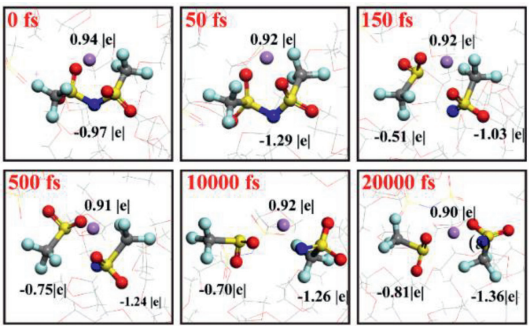

Fig. 2. The LiTFSI initial redox reactions and instantaneous charges (in |e|) from AIMD simulations of S–N situations.

[27–29]. For instance, Chen *et al.* proposed the absorption-to-reaction mechanism to illustrate the decomposition process of DOL/DME on the Li-metal anodes (LMAs) surface [16]. The solvents first adsorbed Li and then decomposed is verified based on multi-scale calculations. In addition, Camacho *et al.* devoted to the effect of extra electrons on the electrolyte decomposition mechanism at LMAs, two types of solvent reduction, *i.e.*, radical attacks and C–O bond cleavage, are distinguished using periodic AIMD simulations [30]. Therefore, density functional theory simulations promise to trace the path of side reactions occurring at LMAs and elucidate the mechanism of electrolyte degradation.

In this work, we explicitly demonstrate electron-rich environment near LMAs accelerates the first step in the decomposition of electrolytes (Fig. 1a). LiTFSI and DOL/DME (Fig. 1b) are chosen to model the actual situations because of the outstanding performance in LMBs. The combination of density functional theory (DFT) and *ab initio* molecular dynamics (AIMD) has led to the discovery of a new mechanism, compared to the single decomposition mechanism previously reported [31]. Two primary decomposition mechanisms (S–N and S–C bond breakage) of the electrolyte have been proposed at the electron-rich environment. LiTFSI is more prone to break S–C bond with the increase of DOL content, while if the proportion of DME is higher, the S–N bond fractures are more likely to occur. In addition, the ratio of DOL/DME has a great effect on the reaction kinetics of Li salts, including fracture time, time for fragments to reach equilibrium, charge transfer, and shedding of F^-. Moreover, the lowest unoccupied molecular orbital (LUMO) energy level [32] of solvation structures is higher by the additional electrons, which enhances the reduction stability of solvation structures formed by the decomposition of the LiTFSI. As a consequence, the processes of the initial stage of electrolyte decomposition are clarified. The current work provides a fundamental understanding of the side reaction that occurs at LMAs and proposes a promising strategy for electrolyte design.

Inspired by the excellent performance of ether electrolyte systems, we study them through computational simulations. The details of building these configurations are in Note 1 (Supporting information). Among the studied electrolyte systems, the salt-involved ones are considered separately compared to the pure solvent ones. The statistics with the additional electron simulation results show that LiTFSI would dissociate in all cases, but the path of fracture varies with the system. For the 1 mol/L LiTFSI/DME mixtures, the situation of S–C bond cleavage predominates. Other situations account for only a small fraction, such as S–C or S–C/S–N bond breakage. Similarly, in 1 mol/L LiTFSI/DOL mixtures, the composition of LiTFSI fragments is more likely to be $CF_3SO_2N^-$ and $CF_3SO_2^-$, and that is the situation of S–N bond breakage. Concerning the more complex 1 mol/L LiTFSI/DME:DOL mixture (1:1, v/v), further investigations are necessary for both situations since the S–C and S–N fracture situations occur uniformly. Overall, seven cases, including pure DME, pure DOL, mixed DME/DOL; 1 mol/L LiTFSI/DME, 1 mol/L LiTFSI/DOL; 1 mol/L LiTFSI/DME:DOL mixture (S–C, denoted as S–C situations), 1 mol/L LiTFSI/DME:DOL mixture (S–N, denoted as S–N situations), are identified with longer AIMD trajectories to obtain more details, whose initial configurations are illustrated in Fig. 1c and d and Fig. S1 (Supporting information).

First, as one of the most common electrolyte systems with excellent performance in experiments [23], salt-bearing systems with mixed solvents are first studied specifically. In previous simulations, two equivalent yet distinct fracture modes (S–N, S–C) appear in the mixed solvent electrolyte system. Regarding the S–N situations, one LiTFSI molecule decomposed (denoted as the first LiTFSI) at the beginning of the AIMD simulation, while the other one remained intact (denoted as the second LiTFSI) until the further addition of electrons. Fig. 2 shows the exact reduction of the decomposed LiTFSI, which started to gain electrons slowly in the early stage of the simulation. It is not until 150 fs that the S–N bond is broken to form $CF_3SO_2^-$ and $CF_3SO_2N^-$, at which point LiTFSI salt gains 0.5|e|. Thereafter, the electrons continue to enter the fragmented components of the LiTFSI. The fragments of $CF_3SO_2^-$ and $CF_3SO_2N^-$ jointly obtained 1|e| at 500 fs, which is maintained until 20,000 fs. The above results indicate that the breakage of the S–N bond is attributed to the sluggish electron gain of LiTFSI, whose charge evolution is almost terminated in the early stage of the simulation. To investigate the charge transfer in more detail, the charge of the electrolyte system is examined *via* Bader charge analysis every 5 fs from 0 to 500 fs (Fig. S2 in Supporting information). It clearly shows the trend that the $CF_3SO_2^-$ and $CF_3SO_2N^-$fragments slowly gets 1|e|. To evaluate the effect of electron concentration on LiTFSI degradation, Table S1 (Supporting information) shows a summary of bond cleavages and fragments after 20 ps in the situation of S–N bond breaks. As the electron concentration increases, the first LiTFSI continues to undergo S–C and C–F bond cleavages, leading to form the fragments $CF_2SO_2N^-$, F^-, CF_3^-, and SO_2^-. While the second LiTFSI breaks in a similar sequence, but without the shedding of F^-.

For a better understanding of the discrepancy caused by breaking the S–C bond, the S–C situations are also inspected in the methods described above. Compared to the S–N situations, the first LiTFSI also gains electrons from the very beginning yet at a faster rate, as depicted in Fig. S3 (Supporting information). Additionally, the fragment from S–C bond breakage, *i.e.*, $CF_3SO_2NSO_2^{2-}$, maintains a charge of −1.4|e| until the end of the simulation, which is somehow dissimilar from the previous case that $CF_3SO_2^-$ and $CF_3SO_2N^-$ require a little time to stabilize their charge. Another fragment, CF_3^-, takes more time in searching for the steady state. Similar to the above S–N situations, the decomposed LiTFSI gains

1|e| at the end of system evolution. As plotted in Fig. S4 (Supporting information), the Bader charge analysis indeed notes the charge of diverse components of the electrolyte system, suggesting that the 1 |e| obtained by the LiTFSI enter $CF_3SO_2NSO_2^{2-}$ and CF_3^- formed by the cleavage of S–C bond. Table S2 (Supporting information) presents the degradation of LiTFSI upon increasing electron concentration. It is found that the first LiTFSI experienced another S–C cleavage in $CF_3SO_2NSO_2^{2-}$ fragments to form two CF_3^- and $SO_2NSO_2^-$. Besides, the second LiTFSI has undergone successive S–N and S–C breaks as a result of varying chemical environments.

Next, we change the proportion of solvents, 1 mol/L LiTFSI/DOL and 1 mol/L LiTFSI/DME electrolyte systems exhibit different primary fracture modes. Unexpectedly, this is corresponding to the fracture pattern of the mixed solvent systems with LiTFSI. Compared with the mixed solvent electrolyte system, the electrolyte environment of pure solvent with salt is relatively simple. Regarding the 1 mol/L LiTFSI/DOL electrolyte system, Fig. S5 (Supporting information) shows that one LiTFSI molecule displays the same bond breaking pattern as the one in S–N situations. However, the difference is that the LiTFSI, which eventually decomposes, experiences a fairly smooth phase in the early stage of the simulation. At 150 fs, the charge of the LiTFSI remains at 0|e|. Thereafter, fragments of $CF_3SO_2^-$ and $CF_3SO_2N^-$ are discovered in the electrolyte at 500 fs. Subsequently, the charge of both fragments only fluctuates around the previously acquired values. For a clearer picture of charge evolution, Fig. S6 (Supporting information) illustrates the charge variation of various components in the electrolyte system. It is not until around 200 fs that these fragments start to gain electrons, undergoing an S–N break from $CF_3SO_2^-$ and $CF_3SO_2N^-$. Interestingly, the first LiTFSI remains stable under the attack of more electrons (Table S3 in Supporting information). Whereas the second LiTFSI undergoes a consistent initial bond breaking (S–N).

To emphasize the discrepancy between different solvent molecules, the initial decomposition of the first LiTFSI in 1 mol/L LiTFSI/DME is shown in Fig. S7 (Supporting information). The behaviors of the impending decomposed LiTFSI are analogous to those of the salts in the mixed solvent electrolyte system. The LiTFSI molecule also gets electrons at the beginning of the simulation. In addition, the charge of LiTFSI fragments stabilizes rapidly after the S–C fracture and persists until the end of the simulation. Compared to S–C situations in mixed solvent, there is a more stable CF_3^- fragment found in 1 mol/L LiTFSI/DME electrolyte system. The following charge evolution diagram (Fig. S8 in Supporting information) could elucidate the above results. As expected, there have been immediate changes in the charge of various parts of the electrolyte system. Table S4 (Supporting information) presents that the two LiTFSI molecules break first in S–C and then in S–N. These results further validate the previous conclusions regarding the influence of the chemical environment on the initial reaction kinetics, which is an electron-rich environment near the interface accelerates the decomposition of electrolytes. The results of pure solvents present in Note 2 (Supporting information).

According to the above AIMD results, we obtained some basic information about the effect of different solvent components and the electron-rich environment on electrolyte degradation. As the proportion of DOL increases, LiTFSI is more prone to break S–C, while if the proportion of DME is higher, the S–N bond breakage is more likely to occur. More importantly, the increasing electron concentration brings about a further decomposition of LiTFSI and accelerates the kinetic rate of decomposition. Although the decomposition products of LiTFSI are almost the same in different electrolyte systems, the F^-, which is more easily shed in the salt-containing system with mixed solvents, has caught our attention and continues to be explored from the perspective of thermodynamic stability in later sections.

The above studies find that Li ions have no charge change during the simulations, while the introduction of Li salts is crucial for the electrolyte system, which has the effect of conducting Li ions giving LMBs the advantages of high voltage, high specific energy [33], *etc*. Inspired by the application of solvation structures in Li-ion batteries, we overcome the shortcomings of implicit solvents in previous work [5,31] and well explain the decomposition behavior of electrolytes through a series of analyzes in solvation structures. Subsequently, we paid more attention to the solvation structures of Li ions by RDF analysis. For the S–N situations, Fig. 3a illustrates the $g(r)$ of Li-O in separate solvent molecules over a 20 ps trajectory. The similarly shaped peaks are observed at a radius of 2.0 Å with a coordination number of 2, indicating that the solvation structures of the electrolyte system is composed of several DME or DOL and $TFSI^-$ at 1.9–2.0 Å In order to investigate more detailed coordination patterns, a conformational analysis of molecules is carried out to reveal the more specific component changes of the solvation structures for a further supplement to RDF. In the electron-rich environment, two different solvation structures exist in the final configuration. Table S5 (Supporting information) presents the calculated Li ions binding energies of the solvation structures. The Li_2 containing solvation structure (denoted as the second solvation structure) has lower binding energy than the Li_1 containing solvation structure (denoted as the first solvation structure). Therefore, it is used as a research object. Table S6 (Supporting information) lists the transformation of Li ion solvation structures in S–N situations for different simulation times. The second solvation structure in table is more consistent with the results of the radial distribution function, its structures shown in Fig. 3b. The transformation process of the solvation structures is shown in Fig. 3c. The solvation structure contains one DME, two DOL and one $TFSI^-$ anion during most of the simulations. The binding form of the DME anion to Li ion converts from one Li ion coordinated with two oxygen atoms (denoted as A-DME, as shown in Fig. 3d) to one Li ion coordinated with one oxygen atom (denoted as B-DME, as shown in Fig. 3e) within 19 ps and eventually stabilized. Based on the current results, it is found that the DME molecule tends to generate A-DME, a kind of DME molecule that is easy to twist, which exposes oxygen atoms with negligible charge.

The effect of an electron-rich environment on solvation structures at the initial stage of the reaction is investigated by AIMD simulation. As shown in Fig. 3f, the coordination number of Li-O_{DME} is significantly reduced and that of Li-O_{DOL} is remarkably increased compared to the cases without excess electrons, suggesting that the solvation structure would consist of more DOL molecules and be accompanied by the desolvation of DME molecules following the conversion of A-DME to B-DME in electron-rich environment. Analogously, a detailed insight into the solvation structures at different times during the simulation is also given in Table S6, where a more specific solvation transition is obtained. Intriguingly, the solvation structure consists of two B-DME molecules, one DOL molecule, and one $TFSI^-$ in contrast to the previous situation. Afterward, one DOL molecule and the fragment $CF_3SO_2^-$ re-entered the solvation structure with the desolvation behavior of one B-DME molecule and one $TFSI^-$. Apparently, the desolvaion of the DME molecule is the main reason for the Li-O_{DME} reduction in coordination number. Fig. 3g shows the solvation structures of S–N situations in electron-rich environment observed from AIMD trajectory. Combining $g(r)$ and the obtained results indicate that a DOL-dominated solvation structure is generated under the effect of electron-rich environment in S–N situations. Finally, the transformation process of the solvation structures are shown in Fig. 3h, and the solvation structures in S–C situations is presented in Note 3 (Supporting information).

To verify the effect of different chemical environment (proportion of DOL to DME) on LiTFSI and solvation structures, 1 mol/L

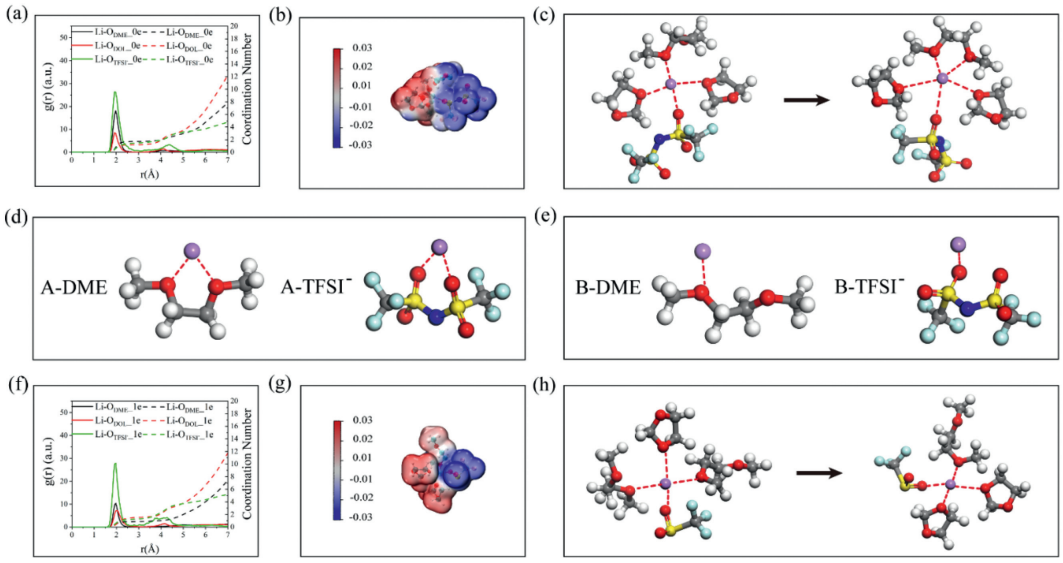

Fig. 3. (a) The radial distribution function of lithium-oxygen interaction (full lines) and relationship between the coordination number and bond distances (short dashed lines) for the S–N situations without excess electrons. (b) The stable solvation structure of S–N situations without excess electrons. (c) The transformation process of the solvation structure in S–N situations without excess electrons. (d) The structure of A-DME, the same for A-TFSI$^-$. (e) The structure of B-DME, the same for B-TFSI$^-$. (f) The radial distribution function of lithium-oxygen interaction and relationship between the coordination number and bond distances for the S–N situations in electron-rich environment. (g) The stable solvation structure of S–N situations in electron-rich environment. (h) The transformation process of the solvation structure in S–N situations in electron-rich environment.

LiTFSI/DOL and 1 mol/L LiTFSI/DME electrolyte systems are investigated in detail by AIMD in two extreme environments. Concerning the circumstances without excess electrons, Fig. S9a (Supporting information) shows the RDF of 1 mol/L LiTFSI/DOL. The coordination number of the Li-O_{DOL} is significantly more than that in the mixed solvent electrolyte systems, around 3. After that, a summary of the transformation of Li ion solvation structures in 1 mol/L LiTFSI/DOL electrolyte system is shown in Table S7 (Supporting information). Table S5 shows the second solvation structure is more stable due to lower binding energy. The solvation structure contains four DOL molecules and one B-TFSI$^-$ at the end of the simulation, which is in good agreement with the results for $g(r)$ above (Fig. S9b in Supporting information).

Likewise, we have investigated the effect of electron-rich environment on the solvation structures for 1 mol/L LiTFSI/DOL electrolyte system. As shown in Fig. S9c (Supporting information), there is a slight decrease in the coordination number of the Li-O_{DOL}, which is definitely caused by the desolvation of DOL molecules due to the excess electrons. To understand the detailed process of solvation transformation, Table S7 shows the transformation of solvation structures in 1 mol/L LiTFSI/DOL electrolyte system in electron-rich environment. Meanwhile, the solvation structure with fragment $CF_3SO_2N^-$ evolves from the unstable state with two DOL molecules and one A-TFSI$^-$ anion. The number of DOL molecules increases to three when the stable state is reached (Fig. S9d in Supporting information). According to the above results, it can be inferred that the effect of electron-rich environment is to violently desolvate the DOL molecules. Yet if the delocalized electron concentration is not high enough, the DOL molecule will re-enter the solvation structure to achieve equilibrium, but it is difficult to return to the initial state. Likewise, the solvation structures that are not completely desolvated will have severe side reactions with Li anodes, resulting in unstable SEI and affecting the battery performance [34,35]. The solvation structures in 1 mol/L LiTFSI/DME electrolyte system are presented in Note 4 (Supporting information).

Through the RDF and conformational analysis of molecules, some preliminary insights into the solvation structures have been obtained. The coordination radius of different solvation structures are kept around 2 Å, while the coordination numbers of the Li-O_{total} in relatively stable solvation structures is either 4 or 5. When the proportion of DOL or DME increased, more of these solvent molecules will enter the solvation structures and desolvate the other kind of solvent molecules in a specific way, forming a specific-solvent-dominated solvation structure that ultimately affects the degradation of the electrolyte. Upon the electron-rich environment, the TFSI$^-$ in the solvation structures are replaced by different salt fragments. Additionally, based on the results of Tables S6-S9 (Supporting information), most B-DME in solvation structures will convert to A-DME without excess electrons because of A-DME tends to distort, trapping Li ions. However, B-TFSI$^-$ is more likely to be presented in solvation structures due to large steric hindrance and negative charge. In the case of electron-rich environments, the B-DME has a better stability in solvation structures under the influence of the background charge polarization. Thus, a conclusion about coordination stability with Li ion emerged: B-TFSI$^-$ > A-TFSI$^-$, A-DME > B-DME for without excess electrons, B-DME > A-DME in electron-rich environment.

Next, we wish to confirm these results from an energetic point of view. To evaluate the case with the degradation of electrolytes, the bond dissociation energies of the TFSI$^-$ are calculated by explicit solvation structures. This approach addresses well the accuracy of implicit solvent dissociation energy calculations previously reports [5,31]. As shown in Fig. 4a, the bond dissociation energy of the TFSI$^-$ for S–N is smaller than that for S–C (3.55 eV *vs.* 3.96 eV) in 1 mol/L LiTFSI/DOL electrolyte system, implying that the LiTFSI is more prone to break S–C in an environment with high DOL proportion. Furthermore, the presence of F$^-$ in mixed solvent electrolyte systems has drawn our attention. Recently, many works have demonstrated that F$^-$ improves the stability of the battery interface and the reduction resistance of electrolytes by generating the LiF phase and changing the Li ion solvation structures [36,37]. Therefore, the possibility of shedding F$^-$ from the initial decomposition products of LiTFSI is explored in this work. According to the results based on bond dissociation energy, CF_3^- has a lower energy barrier of 2.24 eV and thus has more opportunities to shed F$^-$. However, the more easily broken S–N bond makes the possibility of CF_3^- appearance quite low, which explains the poor per-

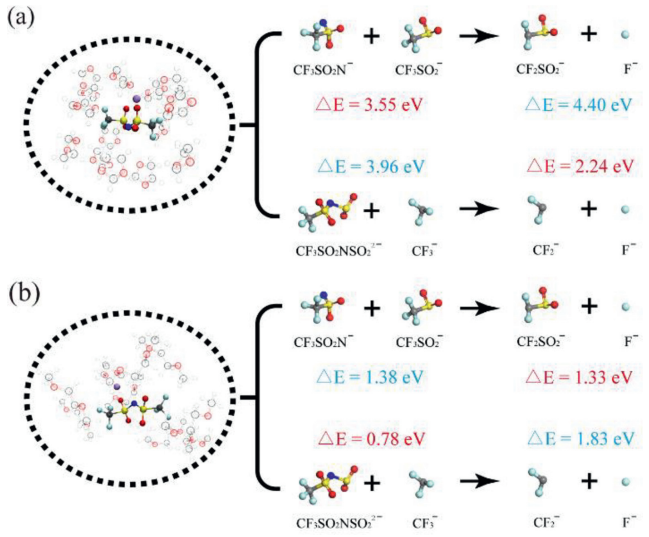

Fig. 4. The bond dissociation energies of different fracture modes for $TFSI^-$ and fragments in explicit solvation structure of (a) 1 mol/L LiTFSI/DOL electrolyte system and (b) 1 mol/L LiTFSI/DME electrolyte system.

formance of the pure solvent electrolyte system in experiments. Concerning 1 mol/L LiTFSI/DME electrolyte system (Fig. 4b), the S–C bond cleavage dominates due to its lower bond dissociation energy (0.78 eV). Similarly, it is easier to produce $CF_3SO_2^-$ but more difficult to produce F^-. All in all, a single electrolyte system results in a single chemical environment that hinder the shedding of F^- and eventually leads to poor battery performance. In contrast, a mixed electrolyte system with diverse chemical environments improved battery performance.

To further understand the effects of different solvation structures on the reduction stability of electrolytes, the frontier molecular orbital theory calculations are performed to evaluate LUMO energy levels of different solvation structures in the studied electrolyte systems. In general, a lower LUMO energy level indicates a higher reduction potential of the molecule. As shown in Fig. 5a, electrolyte systems without excess electrons, the solvation structures in mixed solvent electrolyte systems have similar LUMO energy levels (−0.54 eV and −0.52 eV), with the highest and lowest LUMO energy levels (−0.49 eV and −0.78 eV) being occupied by the solvation structures in pure solvent electrolyte systems (DME, DOL), respectively. It suggests that the LUMO energy levels of the solvation structures decrease with the entry of DOL molecules and increase with the entry of DME molecules. Regarding Fig. 5b, the electrolyte systems in electron-rich environment, the LUMO energy levels of most electrolyte systems are significantly improved, indicating better reduction stability. The results of HOMO energy level are also presented in Figs. S12 and S13 (Supporting information).

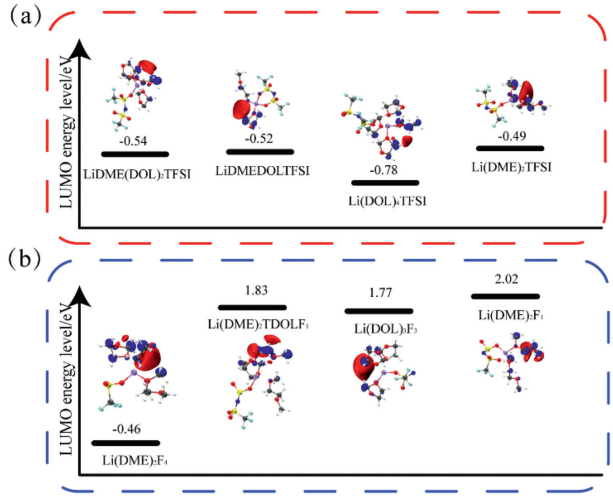

Fig. 5. The visual LUMO energy levels of Li ion solvated structures in different solutions. (a) The electrolyte systems without excess electrons. (b) The electrolyte systems in electron-rich environment. F_1, F_2, F_3 and F_4 represent $CF_3SO_2NSO_2^{2-}$, CF_3^-, $CF_3SO_2N^-$, $CF_3SO_2^-$, respectively. The red and blue isosurfaces represent the orbital wavefunction with opposite directions. (isovalue = 0.025 a.u.).

In summary, we use DFT simulation to investigate the effect of electron-rich environment on the initial decomposition of LiTFSI and the solvation structures transformations in different ether electrolytes near the LMAs interface. In the mixed electrolyte system, excess electrons promote the decomposition of LiTFSI and two primary decomposition mechanisms (S–N and S–C bond breakage) of the LiTFSI are found. With the increase of DOL proportion, the LiTFSI is more prone to break S–C, while if the proportion of DME is higher, the S–N bond breakage is more likely to occur. Furthermore, the proportion of the DME and DOL have a little effect on the final products of LiTFSI decomposition and more on the reaction kinetics of LiTFSI decomposition, including fracture time, time for fragments to reach equilibrium, charge transfer and shedding of F^-, which is utilized to regulate the decomposition of the LiTFSI for construction of SEI with LiF. Likewise, the solvent proportion and electron-rich environment have a certain effect on the solvation structures, involving a certain degree of desolvation and transformation of coordination modes, as in electron-rich environment, the B-DME shows better stability than A-DME, while B-$TFSI^-$ still remains stable. Moreover, affected by the solvent proportion, the entry of DOL into the solvation structures will reduce the LUMO energy level, while the DME will increase the LUMO energy level. Finally, the LUMO energy level would be improved by extra electrons, which enhanced reduction stability of electrolytes formed by LiTFSI fragments. Our study provided new insight on the initial stage of electrolyte degradation mechanisms near the LMAs for further study of complex electrified interfacial reactions to better design the next-generation rechargeable batteries.

Declaration of competing interest

The authors declare that they have no known competing financial interests or personal relationships that could have appeared to influence the work reported in this paper.

Acknowledgments

The authors acknowledge financial support from the National Key Research and Development Project of China (No. 2022YFE0113800), the National Natural Science Foundation of China (Nos. U21A20174, 52225208 and 51972285), the Natural Science Foundation of Zhejiang Province (No. LY23E020010), and the funding of “Leading Innovative and Entrepreneur Team Introduction Program of Zhejiang” (No. 2020R01002). The authors thank Beijing PARATERA Tech Co., Ltd. and Shanghai Hongzhiwei Tech Co., Ltd. for providing HPC resources.

Supplementary materials

Supplementary material associated with this article can be found, in the online version, at doi:10.1016/j.cclet.2023.108510.

References

[1] Y.J. Liu, X.Y. Tao, Y. Wang, et al., Science 375 (2022) 739–745.
[2] Y. He, W. Fan, Y. Zhang, et al., ACS Appl. Mater. Interfaces 12 (2020) 22268–22277.

[3] H. Chen, M. Li, C. Li, et al., Chin. Chem. Lett. 33 (2022) 141–152.
[4] Z.W. Zhang, Y.Z. Li, R. Xu, et al., Science 375 (2022) 66–70.
[5] L.E. C.amacho-Forero, T.W. Smith, P.B. Balbuena, J. Phys. Chem. C 121 (2016) 182–194.
[6] Z.J. Ju, J.W. Nai, Y. Wang, et al., Nat. Commun. 11 (2020) 488.
[7] M.B. Pinson, M.Z. Bazant, J. Electrochem. Soc. 160 (2013) A243–A250.
[8] Y.Z. Li, Y.B. Li, A.L. Pei, et al., Science 358 (2017) 506–510.
[9] J. Wu, M. Ihsan-Ul-Haq, Y. Chen, et al., Nano Energy 89 (2021) 106489.
[10] K. Xu, Chem. Rev. 114 (2014) 11503–11618.
[11] Y. Liu, Z. Yu, J. Chen, et al., Chin. Chem. Lett. 33 (2022) 1817–1830.
[12] X. Shen, P. Li, X. Liu, et al., Chem. Sci. 12 (2021) 9037–9041.
[13] Z. Yu, H. Wang, X. Kong, et al., Nat. Energy 5 (2020) 526–533.
[14] X. Cao, P. Gao, X. Ren, et al., Proc. Natl. Acad. Sci. U. S. A. 118 (2021) e2020357118.
[15] H. Cheng, Q. Sun, L. Li, et al., ACS Energy Lett. 7 (2022) 490–513.
[16] X. Chen, T.Z. Hou, B. Li, et al., Energy Storage Mater. 8 (2017) 194–201.
[17] W. Chen, C.X. Zhao, B. Li, et al., Energy Environ. Mater. 3 (2020) 160–165.
[18] P.B. Zhai, L.X. Liu, X.K. Gu, et al., Adv. Energy Mater. 10 (2020) 2001257.
[19] X.Q. Zhang, X.B. Cheng, X. Chen, et al., Adv. Funct. Mater. 27 (2017) 10–1605958.
[20] L. Suo, Y.S. Hu, H. Li, et al., Nat. Commun. 4 (2013) 1481.
[21] J. Qian, W.A. Henderson, W. Xu, et al., Nat Commun. 6 (2015) 6362.
[22] X. Chen, Q. Zhang, Acc. Chem. Res. 53 (2020) 1992–2002.
[23] L.X. Li, R. Li, Z.H. Huang, et al., Colloid. Surf. A 651 (2022) 129665.
[24] D. Xiao, Q. Li, D. Luo, et al., Small 16 (2020) e2004688.
[25] P. Zou, Y. Sui, H. Zhan, et al., Chem. Rev. 121 (2021) 5986–6056.
[26] G. Zhou, S. Zhao, T. Wang, et al., Nano Lett. 20 (2020) 1252–1261.
[27] Y. Wang, Q.F. Xie, J.H. Zhang, et al., Comput. Mater. Sci. 211 (2022) 111523.
[28] J.H. Zheng, Z.J. Ju, B.L. Zhang, et al., J. Mater. Chem. A 9 (2021) 10251–10259.
[29] C. Sun, M. Liu, L. Wang, et al., Chin. Chem. Lett. 33 (2022) 1779–1797.
[30] L.E. Camacho-Forero, P.B. Balbuena, J. Power Sources 472 (2020) 228449.
[31] L.E. Camacho-Forero, T.W. Smith, S. Bertolini, J. Phys. Chem. C 119 (2015) 26828–26839.
[32] K. Houk, Acc. Chem. Res. 7 (1975) 361–369.
[33] E. Peled, S. Menkin, J. Electrochem. Soc. 164 (2017) A1703–A1719.
[34] J.M. Zhang, Q.P. Li, Y.P. Zeng, et al., ACS Energy Lett. 8 (2023) 1752–1761.
[35] D.J. Xiao, Q. Li, D. Luo, et al., Small 16 (2020) e2004688.
[36] M. Chen, J.H. Zheng, Y.J. Liu, et al., Adv. Funct. Mater. 31 (36) (2021) 2102228.
[37] J.H. Zheng, Y. Wang, J.C. Wang, et al., ACS Appl. Mater. Interfaces 14 (2022) 48762–48769.